

Pair winds in Schwarzschild space-time with application to hot bare strange stars

A.G. Aksenov ¹, M. Milgrom, V.V. Usov

Center for Astrophysics, Weizmann Institute, Rehovot 76100, Israel

ABSTRACT

We consider a time dependent, spherically outflowing wind, in Schwarzschild space-time, consisting of electron-positron pairs and photons. Without assuming thermal equilibrium, we account for the microphysics, including two-body processes ($ee \rightarrow ee$, $\gamma e \rightarrow \gamma e$, $e^+e^- \leftrightarrow \gamma\gamma$) and their radiative three-body variants ($ee \leftrightarrow ee\gamma$, $\gamma e \leftrightarrow \gamma e\gamma$, $e^+e^- \leftrightarrow \gamma\gamma\gamma$). We present a finite-difference scheme for solving the general relativistic kinetic Boltzmann equations for pairs and photons. We apply this to the concrete example of a wind from a hot, bare, strange star, predicted to be a powerful source of hard X-ray photons and e^\pm pairs created by the Coulomb barrier at the quark surface. We study the kinetics of the wind particles and the emerging emission in photons and pairs for stationary winds with total luminosities in the range $10^{34} - 10^{39}$ ergs s^{-1} , for different values of the injected photon-to-pair ratio. The wind parameters—such as the mean optical depth for photons, the rates of particle number and energy outflows, bulk velocity, and number density of the pair plasma—are presented as functions of the distance from the stellar surface, as well as characteristics of the emergent radiation. We find that photons dominate in the emerging emission, and the emerging photon spectrum is rather hard and differs substantially from the thermal spectrum expected from a neutron star with the same luminosity. This might help distinguish the putative bare strange stars from neutron stars.

Subject headings: radiation mechanisms: thermal — plasmas — X-rays: stars — radiative transfer — stars: neutron

¹Institute of Theoretical and Experimental Physics, B. Cheremushkinskaya, 25, Moscow 117259, Russia; Alexei.Aksenov@itep.ru

1. Introduction

Compact astronomical objects identified with neutron stars, strange stars, and black holes are believed to be sources of electron-positron (e^\pm) pairs that form in their vicinity by different mechanisms and flow away. Among these objects are radio pulsars (Sturrock 1971, Ruderman & Sutherland 1975, Arons 1981; Usov & Melrose 1996; Baring & Harding 2001), accretion-disc coronas of the Galactic X-ray binaries (White & Lightman 1989; Sunyaev et al. 1992), soft γ -ray repeaters (Thompson & Duncan 1995; Usov 2001b), cosmological γ -ray bursters (Eichler et al. 1989; Paczyński 1990; Usov 1992), etc.. The estimated luminosity in e^\pm pairs varies greatly depending on the object and the specific conditions: from $\sim 10^{31} - 10^{35}$ ergs s^{-1} or less for radio pulsars up to $\sim 10^{50} - 10^{52}$ ergs s^{-1} in cosmological γ -ray bursters.

For a wind out-flowing spherically from a surface of radius R there is a maximum (isotropic, unbeamed) pair luminosity beyond which the pairs annihilate significantly before they escape (see Beloborodov 1999 and references therein). This is given by

$$L_{\pm}^{\max} = \frac{4\pi m_e c^3 R \Gamma^2}{\sigma_T} \simeq 10^{36} (R/10^6 \text{ cm}) \Gamma^2 \text{ ergs s}^{-1}, \quad (1)$$

where Γ is the pair bulk Lorentz factor, and σ_T the Thomson cross section. When the injected pair luminosity, \tilde{L}_{\pm} , greatly exceeds this value the emerging pair luminosity, L_{\pm} , cannot significantly exceed L_{\pm}^{\max} ; in this case photons strongly dominate in the emerging emission: $L_{\pm} \lesssim L_{\pm}^{\max} \ll \tilde{L}_{\pm} \simeq L_{\gamma}$. Injected pair luminosities typical of cosmological γ -ray bursts (e.g., Piran 2000), $\tilde{L}_{\pm} \sim 10^{50} - 10^{52}$ ergs s^{-1} , greatly exceed L_{\pm}^{\max} for their estimated $\Gamma_{\pm} \sim 10^2$. For such a powerful wind the pair density near the source is very high, and the out-flowing pairs and photons are nearly in thermal equilibrium almost up to the wind photosphere (e.g., Paczyński 1990). The outflow process of such a wind may be described fairly well by relativistic hydrodynamics (Paczyński 1986, 1990; Goodman 1986; Grimsrud & Wasserman 1998; Iwamoto & Takahara 2002).

In contrast if $\tilde{L}_{\pm} \ll L_{\pm}^{\max}$ annihilation of the outflowing pairs is negligible. It is now commonly accepted that the magnetospheres of radio pulsars contain such a very rarefied ultra-relativistic ($\Gamma_{\pm} \sim 10 - 10^2$) pair plasma that is practically collisionless (see Melrose 1995 for a review).

Recently we described a numerical code and the results of calculations of spherically out-flowing, non-relativistic ($\Gamma_{\pm} \sim 1$) pair winds with total luminosity in the range $10^{34} - 10^{42}$ ergs s^{-1} , that is $L \sim (10^{-2} - 10^6) L_{\pm}^{\max}$ (Aksenov, Milgrom, & Usov 2004, hereafter Paper I). (A brief account of the emerging emission from such a pair wind has been given by Aksenov Milgrom & Usov 2003.) While our numerical code can be more generally employed, the results we presented in Paper I were for a hot, bare, strange star as the a wind injection

source. Such stars are thought to be powerful sources of pairs created by the Coulomb barrier at the quark surface (Usov 1998, 2001a, see Fig. 1). For such luminosities it is not justified to assume thermal equilibrium, and so we have calculated the detailed microphysics including all two-body processes ($ee \rightarrow ee$, $\gamma e \rightarrow \gamma e$, $e^+e^- \leftrightarrow \gamma\gamma$) as well as their radiative three-body variants ($ee \leftrightarrow ee\gamma$, $\gamma e \leftrightarrow \gamma e\gamma$, $e^+e^- \leftrightarrow \gamma\gamma\gamma$). The relativistic kinetic Boltzmann equations for pairs and photons were solved numerically to describe the time evolution and structure of pair winds and to find the emergent emission (we only presented results for stationary situations). Gravity of the star was neglected, and it was assumed that only e^\pm pairs are emitted from the stellar surface. Thermal emission of photons from a bare quark surface, which has been neglected in Paper I, is strongly suppressed relative to black-body emission, but not completely, (e.g., Cheng & Harko 2003; Jaikumar et al. 2004, see Fig. 1). Still, whatever little is emitted may significantly affect the wind properties (see below).

In the present paper we extend our previous studies to also include the effects of gravity by solving the Boltzmann equations for pairs and photons in a Schwarzschild space-time appropriate for the strange star. We also include thermal emission of photons from the stellar surface.

In § 2 we formulate the equations that describe the pair wind and the boundary conditions. In § 3 we describe the computational method used to solve these equations. In § 4 we present the results of our numerical simulations. Finally, in § 5, we discuss our results and some potential astrophysical applications.

2. Formulation of the problem

We consider an e^\pm pair wind that flows away from a hot, bare, unmagnetized, non-rotating, strange star. Space-time outside the star is described by Schwarzschild’s metric with the line element

$$ds^2 = -e^{2\phi}c^2dt^2 + e^{-2\phi}dr^2 + r^2(d\theta^2 + \sin^2\theta d\varphi^2), \quad (2)$$

where

$$e^\phi = (1 - r_g/r)^{1/2} \quad (3)$$

is the lapse or redshift factor induced by gravity at a distance r from the stellar center,

$$r_g = 2GM/c^2 \simeq 2.95 \times 10^5 M/M_\odot \text{ cm} \quad (4)$$

is the gravitational radius, with M the gravitational mass of the star.

Following Page & Usov (2002) we consider, as a representative case, a strange star with $M = 1.4M_\odot$ which is constructed by solving the Tolman-Oppenheimer- Volkoff equation of hydrostatic equilibrium using an equation of state for SQM as described in Alcock, Farhi, & Olinto (1986a) and in Haensel, Zdunik, & Schaefer (1986) [with a bag constant $B = (140\text{MeV})^4$, QCD coupling constant $\alpha_c \equiv g^2/4\pi = 0.3$, and the mass of strange quarks $m_s = 150 \text{ MeV}$]. The circumferential radius of the star is $R = 1.1 \times 10^6 \text{ cm}$.

We assume that the temperature is constant over the surface of the star. The thermal emission in pairs and photons from the surface of strange quark matter (SQM) depends on the surface temperature, T_S , alone (Usov 1998, 2001a; Cheng & Harko 2003; Jaikumar et al. 2004). The state of the plasma in the wind may be described by the distribution functions $f_\pm(\mathbf{p}, r, t)$ and $f_\gamma(\mathbf{p}, r, t)$ for positrons (+), electrons (−), and photons, respectively, where \mathbf{p} is the momentum of particles. There is no emission of nuclei from the stellar surface, so the distribution functions of positrons and electrons are identical, $f_+ = f_-$.

Since we fix the mass and radius of the central star the only remaining parameters that determine the wind are the surface temperature, which determines the pair injection rate and spectrum, and the photon surface radiation, which for default of better knowledge we take to be thermal with a suppression factor, η , relative to black body; η is our second free parameter. Because of the very steep dependence of the pair injection rate on the surface temperature, we actually use the former as a free parameter: in our calculations here $\tilde{L}_\pm = 10^{34}, 10^{35}, \dots, 10^{39} \text{ ergs s}^{-1}$.

2.1. General Relativistic Boltzmann Equations

The Boltzmann equations in a Schwarzschild background for either massless or massive particles can be obtained as a special case from the results of Harleston & Holcomb (1991) and Harleston & Vishniac (1992). These are given in a conservative form, which makes them particularly amenable to numerical treatment:

$$\begin{aligned} & \frac{e^{-\phi}}{c} \frac{\partial f_i}{\partial t} + \frac{1}{r^2} \frac{\partial}{\partial r} (r^2 \mu e^\phi \beta_i f_i) - \frac{e^\phi}{p^2} \frac{\partial}{\partial p} \left(p^3 \mu \frac{\phi'}{\beta_i} f_i \right) \\ & - \frac{\partial}{\partial \mu} \left[(1 - \mu^2) e^\phi \left(\frac{\phi'}{\beta_i} - \frac{\beta_i}{r} \right) f_i \right] = \sum_q (\bar{\eta}_i^q - \chi_i^q f_i). \end{aligned} \quad (5)$$

Here, i is the species type ($i = e$ for e^\pm pairs and $i = \gamma$ for photons), $\mu = \cos \theta$, θ is the angle between the radius-vector \mathbf{r} from the stellar center and the particle momentum \mathbf{p} , $p = |\mathbf{p}|$, $\beta_e = v_e/c = [1 - (m_e c^2/\epsilon_e)^2]^{1/2}$, $\beta_\gamma = 1$, and $\epsilon_e = c[p^2 + (m_e c)^2]^{1/2}$ is the energy of electrons and positrons (for photons $\epsilon_\gamma = pc$). Also, $\bar{\eta}_i^q$ is the emission coefficient for the production

of a particle of type i via the physical process labelled by q , and χ_i^q is the corresponding absorption coefficient. The summation runs over physical processes that involve a particle of type i .

For convenience of numerical simulations we use instead of f_i the quantities

$$E_i(\epsilon, \mu, r, t) = \frac{2\pi\epsilon^3\beta_i f_i}{c^3}, \quad (6)$$

standardly used in the “conservative” numerical method. This can provide exact conservation of energy on a finite computational grid (see below). E_i is the energy density in the $\{\mathbf{r}, \mu, \epsilon\}$ phase space. Since all equations are the same for all particle species from now on we omit the index i .

From equations (5) and (6) the Boltzmann equations can be written in terms of E as

$$\begin{aligned} & \frac{e^{-\phi}}{c} \frac{\partial E}{\partial t} + \mu e^{-\phi} \frac{\partial}{r^2 \partial r} (r^2 \beta e^{2\phi} E) - \mu e^{\phi} \phi' \frac{\partial}{\partial \epsilon} (\epsilon \beta E) \\ & - e^{\phi} \frac{\partial}{\partial \mu} \left[(1 - \mu^2) \left(\frac{\phi'}{\beta} - \frac{\beta}{r} \right) E \right] = \sum_q (\eta^q - \chi^q E), \end{aligned} \quad (7)$$

where

$$\eta^q = \frac{2\pi\epsilon^3\beta\eta^q}{c^3}. \quad (8)$$

2.2. Boundary conditions

The computational boundaries are

$$R < r < r_{\text{ext}}, \quad 0 < t < t_{\text{st}}, \quad (9)$$

where $r_{\text{ext}} = 1.66 \times 10^8$ cm, and t_{st} is the time when the wind approaches stationarity close enough, since here we concentrate on steady-state winds.

Considering the interior of the quark star, it was shown that a thin ($\sim 10^{-10}$ cm) layer of electrons with an extremely strong electric field—the electrosphere—forms at the surface of strange quark matter (SQM) (Alcock et al. 1986a; Kettner et al. 1995), which prevents the electrons from escaping to infinity. The electric field in the electrosphere is a few ten times higher than the critical field, $E_{\text{cr}} \simeq 1.3 \times 10^{16}$ V cm $^{-1}$, at which the vacuum is unstable to creation of e^+e^- pairs (Schwinger 1951). Therefore, a hot, bare strange star is potentially a powerful source of e^+e^- pairs created in the electrosphere and flowing away from the star (Usov 1998). We use in our simulations a pair injection rate (Usov 2001a):

$$\dot{N}_{\pm}^{\text{in}} = 4\pi R^2 F_{\pm}, \quad (10)$$

where

$$F_{\pm} = 3 \times 10^{42} \exp(-0.593\zeta) \times \left[\frac{\ln(1 + 2\zeta^{-1})}{(1 + 0.074\zeta)^3} + \frac{\pi^5 \zeta}{2(13.9 + \zeta)^4} \right] \text{ cm}^{-2} \text{ s}^{-1}, \quad (11)$$

and $\zeta = 20(T_S/10^9 \text{ K})^{-1}$. The energy spectrum of injected pairs is thermal with the surface temperature T_S , and their angular distribution is isotropic for $0 \leq \mu \leq 1$.

Thus, the pair injection luminosity, our first free parameter, is given by

$$\tilde{L}_{\pm} = \dot{N}_{\pm}^{\text{in}} [m_e c^2 + (3/2)k_B T_S], \quad (12)$$

where k_B is the Boltzmann constant (Usov 2001a). For the range we consider, $\tilde{L}_{\pm} = 10^{34} - 10^{39} \text{ ergs s}^{-1}$, the surface temperature is in a rather narrow range, $T_S \simeq (4 - 6) \times 10^8 \text{ K}$ (see Fig. 1).

Thermal emission of photons from the surface of a bare strange star is strongly suppressed if the surface temperature is not very high, $T_S \ll 10^{11} \text{ K}$ (Alcock et al. 1986a). The reason is that the plasma frequency of quarks in SQM is very large, $\hbar\omega_p \simeq 20 - 25 \text{ MeV}$, and only hard photons with energies $\epsilon_{\gamma} > \hbar\omega_p$ can propagate in the SQM. The luminosity in such hard photons, which are in thermodynamic equilibrium with quarks, decreases very fast for $T_S \ll \hbar\omega_p/k_B$ (Chmaj, Haensel, & Slomiński 1991; Usov 2001a) and in our case, where $T_S \lesssim 10^9 \text{ K}$, it is negligible (see Fig. 1). However, low-energy ($\epsilon_{\gamma} < \hbar\omega_p$) photons may still leave the SQM if they are produced by nonequilibrium processes in the surface layer of thickness $\sim c/\omega_p \sim 10^{-12} \text{ cm}$ (Chmaj et al. 1991). The emissivity of SQM in nonequilibrium quark-quark bremsstrahlung radiation has been estimated by Cheng & Harko (2003) who find that it is suppressed at least by a factor of 10^6 in comparison with black-body emission, $\tilde{L}_{\gamma} \lesssim 10^{-6} L_{\text{bb}}$. Usov (2004) and Usov, Harko, & Cheng (2005) have recently considered a modified model of the electrosphere taking into account surface effects for SQM. The modification of the electrosphere results in an increase in the density of electrons by a factor of $\sim 20 - 30$ in comparison with the case when the surface effects are ignored. The electron density increase can additionally suppress the outgoing radiation from SQM in nonequilibrium quark-quark bremsstrahlung photons. In our simulations we take

$$\tilde{L}_{\gamma} = \eta L_{\text{bb}} = \eta 4\pi\sigma R^2 T_S^4, \quad (13)$$

where η is a dimensionless free parameter. We present results with $\eta = 0, 3 \times 10^{-8}, 10^{-6}$. In default of better knowledge the photon spectrum is taken as black-body with the surface temperature T_S corresponding to \tilde{L}_{\pm} .

An important parameter characterizing the affect of photon emission from the surface on the out-flowing wind is the Eddington luminosity L_{Edd}^{\pm} for the pair plasma, above which the radiation pressure force dominates over gravity,

$$L_{\text{Edd}}^{\pm} \simeq 10^{35} (M/1.4M_{\odot}) \text{ ergs s}^{-1}. \quad (14)$$

Within the narrow range of surface temperatures studied here, $T_{\text{S}} \simeq (4 - 6) \times 10^8 \text{ K}$, we get \tilde{L}_{γ} that is $\sim (1 - 10)L_{\text{Edd}}^{\pm}$ for $\eta = 3 \times 10^{-8}$, and $\sim (10^2 - 10^3)L_{\text{Edd}}^{\pm}$ for $\eta = 10^{-6}$ (see Fig. 1).

The stellar surface is assumed to be a perfect mirror for both e^{\pm} pairs and photons. At the external boundary ($r = r_{\text{ext}}$) pairs and photons escape freely from the studied region, i.e., the inward ($\mu < 0$) fluxes of both e^{\pm} pairs and photons vanish there.

2.3. Physical processes in the pair plasma

As the plasma moves outwards photons are produced by pair annihilation ($e^+e^- \rightarrow \gamma\gamma$). Other two-body processes that occur in the outflowing plasma, and are included in the simulations, are Møller ($e^+e^+ \rightarrow e^+e^+$ and $e^-e^- \rightarrow e^-e^-$) and Bhaba ($e^+e^- \rightarrow e^+e^-$) scattering, Compton scattering ($\gamma e \rightarrow \gamma e$), and photon-photon pair production ($\gamma\gamma \rightarrow e^+e^-$).

Two-body processes do not change the total number of particles in the system, and thus cannot in themselves lead to thermal equilibrium. So, we also include radiative processes (bremsstrahlung, double Compton scattering, and three-photon annihilation with their inverse processes), even though their cross-sections are at least $\sim \alpha^{-1} \sim 10^2$ times smaller than those of the two-body processes ($\alpha = e^2/\hbar c = 1/137$ is the fine structure constant).

3. The computational method

Our grid in the $\{\mathbf{r}, \mu, \epsilon\}$ phase-space is defined as follows. The r domain ($R < r < r_{\text{ext}}$) is divided into j_{max} spherical shells whose boundaries are designated with half integer indices. The j shell ($1 \leq j \leq j_{\text{max}}$) is between $r_{j-1/2}$ and $r_{j+1/2}$, with $\Delta r_j = r_{j+1/2} - r_{j-1/2}$ ($r_{1/2} = R$ and $r_{j_{\text{max}}+1/2} = r_{\text{ext}}$).

The μ -grid is made of k_{max} intervals $\Delta\mu_k = \mu_{k+1/2} - \mu_{k-1/2}$: $1 \leq k \leq k_{\text{max}}$.

The energy grids for photons and electrons are both made of ω_{max} energy intervals $\Delta\epsilon_{\omega} = \epsilon_{\omega+1/2} - \epsilon_{\omega-1/2}$: $1 \leq \omega \leq \omega_{\text{max}}$, but the lowest energy for photons is 0, while that for pairs is $m_e c^2$.

The quantities we compute are the energy densities averaged over phase-space cells

$$E_{\omega,k,j}(t) = \frac{1}{\Delta X} \int_{\Delta\epsilon_\omega, \Delta\mu_k, \Delta r_j} E d\epsilon d\mu r^2 dr. \quad (15)$$

where $\Delta X = \Delta\epsilon_\omega \Delta\mu_k \Delta(r_j^3)/3$ and $\Delta(r_j^3) = r_{j+1/2}^3 - r_{j-1/2}^3$.

Replacing the space, angle, and energy derivatives in the Boltzmann equations (7) by finite differences (e.g., Mezzacappa & Bruenn 1993) we have the following set of ordinary differential equations (ODEs) for $E_{\omega,k,j}$ specified on the computational grid:

$$\begin{aligned} & \frac{e^{-\phi_j}}{c} \frac{dE_{\omega,k,j}}{dt} + e^{-\phi_j} \beta_\omega \frac{\Delta(r^2 \mu_k e^{2\phi} E_{\omega,k})_j}{\Delta(r_j^3)/3} \\ & - \mu_k e^{\phi_j} \phi'_j \frac{\Delta(\epsilon \beta E_{k,j})_\omega}{\Delta\epsilon_\omega} - e^{\phi_j} \left(\frac{\phi'_j}{\beta_\omega} - \left\langle \frac{1}{r} \right\rangle_j \beta_\omega \right) \\ & \times \frac{\Delta[(1 - \mu^2) E_{\omega,j}]_k}{\Delta\mu_k} = \sum_q [\eta_{\omega,k,j}^q - (\chi E)_{\omega,k,j}^q], \end{aligned} \quad (16)$$

where

$$\beta_\omega = \begin{cases} 1 & \text{for photons,} \\ [1 - (m_e c^2 / \epsilon_\omega)^2]^{1/2} & \text{for electrons,} \end{cases} \quad (17)$$

$$\epsilon_\omega = \frac{\epsilon_{\omega-1/2} + \epsilon_{\omega+1/2}}{2}, \quad (18)$$

$$\mu_k = \frac{\mu_{k-1/2} + \mu_{k+1/2}}{2}, \quad (19)$$

$$r_j = \frac{r_{1-1/2} + r_{j+1/2}}{2}. \quad (20)$$

$$\phi_j = \phi(r_j), \quad \phi'_j = \phi'(r_j) \quad (21)$$

$$\left\langle \frac{1}{r} \right\rangle_j = \frac{(r_{j+1/2}^2 - r_{j-1/2}^2)/2}{(r_{j+1/2}^3 - r_{j-1/2}^3)/3}, \quad (22)$$

$$E_{\omega,k}(r) = \frac{1}{\Delta\epsilon_\omega \Delta\mu_k} \int_{\Delta\epsilon_\omega \Delta\mu_k} E(\epsilon, \mu, r) d\epsilon d\mu, \quad (23)$$

$$E_{\omega,j}(\mu) = \frac{3}{\Delta\epsilon_\omega \Delta r_j^3} \int_{\Delta\epsilon_\omega \Delta r_j} E(\epsilon, \mu, r) dr d\epsilon, \quad (24)$$

$$E_{k,j}(\epsilon) = \frac{3}{\Delta\mu_k \Delta r_j^3} \int_{\Delta\mu_k \Delta r_j^3} E(\epsilon, \mu, r) dr d\mu, \quad (25)$$

$$\begin{aligned} \Delta(r^2 \mu_k e^{2\phi} E_{\omega,k})_j &= r_{j+1/2}^2 e^{2\phi_{j+1/2}} (\mu_k E_{\omega,k})_{r=r_{j+1/2}} \\ &\quad - r_{j-1/2}^2 e^{2\phi_{j-1/2}} (\mu_k E_{\omega,k})_{r=r_{j-1/2}}, \end{aligned} \quad (26)$$

$$\begin{aligned} \Delta (\epsilon \beta E_{k,j})_{\omega} &= \epsilon_{\omega+1/2} \beta_{\omega+1/2} (E_{k,j})_{\omega+1/2} \\ &\quad - \epsilon_{\omega-1/2} \beta_{\omega-1/2} (E_{k,j})_{\omega-1/2}, \end{aligned} \quad (27)$$

$$\begin{aligned} \Delta [(1 - \mu^2) E_{\omega,j}]_k &= (1 - \mu_{k+1/2}^2) (E_{\omega,j})_{\mu=\mu_{k+1/2}} \\ &\quad - (1 - \mu_{k-1/2}^2) (E_{\omega,j})_{\mu=\mu_{k-1/2}}, \end{aligned} \quad (28)$$

$$(E_{k,j})_{\omega+1/2} = \begin{cases} E_{\omega+1,k,j} \\ + \frac{(E_{\omega+2,k,j} - E_{\omega+1,k,j})(\epsilon_{\omega+1/2} - \epsilon_{\omega+1})}{\epsilon_{\omega+2} - \epsilon_{\omega+1}}, \\ \mu \geq 0 \\ E_{\omega,k,j} \\ + \frac{(E_{\omega,k,j} - E_{\omega-1,k,j})(\epsilon_{\omega+1/2} - \epsilon_{\omega})}{\epsilon_{\omega} - \epsilon_{\omega-1}}, \\ \mu < 0, \end{cases} \quad (29)$$

$$\begin{aligned} (E_{\omega,j})_{\mu=\mu_{k+1/2}} &= E_{\omega,k,j} \\ + \frac{\Delta \mu_k (E_{\omega,k,j} - E_{\omega,k-1,j})}{\Delta \mu_{k-1} + \Delta \mu_k}, \end{aligned} \quad (30)$$

$$\begin{aligned} (\mu_k E_{\omega,k})_{r=r_{j+1/2}} &= (1 - \tilde{\chi}_{\omega,k,j+1/2}) \\ \times \left(\frac{\mu_k + |\mu_k|}{2} E_{\omega,k,j} + \frac{\mu_k - |\mu_k|}{2} E_{\omega,k,j+1} \right) \\ + \tilde{\chi}_{\omega,k,j+1/2} \mu_k \frac{E_{\omega,k,j} + E_{\omega,k,j+1}}{2}, \end{aligned} \quad (31)$$

$$\tilde{\chi}_{\omega,k,j+1/2}^{-1} = 1 + \frac{1}{\chi_{\omega,k,j} \Delta r_j} + \frac{1}{\chi_{\omega,k,j} \Delta r_{j+1}}. \quad (32)$$

The dimensionless coefficient $\tilde{\chi}$ is introduced to describe correctly both optically thin and optically thick computational cells by means of a compromise between the high order method and the monotonic transport scheme without the artificial viscosity (e.g., Richtmeyer & Morton 1967; Mezzacappa & Bruenn 1993; Aksenov 1998). It is worth noting that if the values of $(E_{k,j})_{\omega+1/2}$ and $(E_{\omega,j})_{\mu=\mu_{k+1/2}}$ calculated by equations (29) and (30), respectively, are negative they are taken to be zero.

The right side terms of equation (16) are

$$\eta_{\omega,k,j}^q = \frac{1}{\Delta X} \int_{\Delta \epsilon_{\omega}, \Delta \mu_k, \Delta r_j} \eta^q d\epsilon d\mu r^2 dr. \quad (33)$$

$$(\chi E)_{\omega,k,j}^q = \frac{1}{\Delta X} \int_{\Delta\epsilon_\omega, \Delta\mu_k, \Delta r_j} \chi E^q d\epsilon d\mu r^2 dr. \quad (34)$$

For the physical processes included in our simulations expressions $\eta_{\omega,k,j}^q$ and $(\chi E)_{\omega,k,j}^q$ are calculated in Paper I.

In paper I, where gravity is neglected, particle number is explicitly conserved when only two-body processes are taken into account; particle production occurs only via three-body processes. In the general relativistic scheme developed in this paper we were not able to achieve exact number conservation. However, in all runs for a stationary solution the change of the particle flux due to computational effects is at most a few percents. Energy conservation is still exactly satisfied.

There are several characteristic times in the system. Some are related to particle reaction times, some to the time to reach steady state. These times may greatly differ from each other, especially at high luminosities ($\gtrsim 10^{38}$ ergs s⁻¹) when the pair wind is optically thick. The set of equations (16) is then stiff: at least some eigenvalues of the Jacobi matrix differ significantly from each other, and the real parts of the eigenvalues are negative. In contrast to Mezzacappa & Bruenn (1993) we use Gear’s method (Hall & Watt 1976) to solve the ODEs finite differences analog (16) of the Boltzmann equations. This high-order, implicit method was developed especially to find a solution of stiff sets of ODE. To solve a system of linear algebraic equations at any time step of Gear’s method we use the cyclic reduction method (Mezzacappa & Bruenn 1993). The number of operations per time step is $\propto (\omega_{\max} k_{\max})^3 j_{\max}$, which increases rapidly with the increase of ω_{\max} and k_{\max} . Therefore, the numbers of energy and angle intervals have to be rather limited in our simulations.

Here we use an (ϵ, μ, r) -grid with $\omega_{\max} = 13$, $k_{\max} = 8$, and $j_{\max} = 100$. The discrete energies (in keV) of the ϵ -grid minus the rest mass of the particles are 0, 2, 27, 111, 255, 353, 436, 491, 511, 530, 585, 669, 766, and ∞ . This gives a denser grid at low energies and near the threshold of pair production, $\epsilon = m_e c^2$. The μ -grid is uniform, with $\Delta\mu_k = 2/k_{\max} = 1/4$. The shell thicknesses are geometrically spaced: $\Delta r_1 = 2 \times 10^{-4}$ cm, and $\Delta r_j = 1.3 \Delta r_{j-1}$.

To check the effects of grid coarseness we also performed test computations with $k_{\max} = 4$ and 6, and separately with $\omega_{\max} = 10$ and 11. We did not observe changes in the results.

4. Numerical results

In this section, we give the results for the properties of spherically symmetric winds consisting of e^\pm pairs and photons. The pair injection luminosity \tilde{L}_\pm and η are the parameters in our simulations. The photon injection luminosity \tilde{L}_γ is determined by equation (13) where

the surface temperature T_S relates to the value of \tilde{L}_\pm [see equations (10) - (12)]. We start from an empty wind, injecting both pairs at a rate 10^{34} ergs s $^{-1}$ and photons at a corresponding rate. After a steady state is reached we start a new run with this steady state as initial condition, increase the energy injection rate in pairs by a factor of 10, wait for steady state, and so on.

We next present the results for the structure of the stationary winds and their emergent emission at the external boundary.

Figure 2 shows the mean optical depth $\tau_\gamma(r)$ for photons, from r to r_{ext} . The wind as a whole is optically thick [$\tau_\gamma(R) > 1$] for $\tilde{L}_\pm \gtrsim 10^{37}$ ergs s $^{-1}$ irrespective of η . For $\tilde{L}_\pm = 10^{39}$ ergs s $^{-1}$ the radius of the wind photosphere r_{ph} , determined by condition $\tau(r_{\text{ph}}) = 1$, is $\sim 4 \times 10^6$ cm (see Fig. 2). The wind photosphere is always deep inside our chosen external boundary ($r_{\text{ph}} \ll r_{\text{ext}}$), justifying our neglect of the inward ($\mu < 0$) fluxes at $r = r_{\text{ext}}$.

Figures 3 and 4 show the pair number density (n_e) and the bulk velocity of the pair plasma outflow (v_e^{out}), respectively, as functions of the distance from the stellar surface. For high luminosities ($\tilde{L}_\pm \gtrsim 10^{37}$ ergs s $^{-1}$) both these quantities hardly depend on η , i.e., the pair wind structure is determined only by \tilde{L}_\pm . For low luminosities ($\tilde{L}_\pm \lesssim 10^{35}$ ergs s $^{-1}$), n_e and v_e^{out} depend significantly on η . In particular, for $\tilde{L}_\pm = 10^{34}$ ergs s $^{-1}$ near the stellar surface ($r - R \lesssim 10^5$ cm) the pair density for $\eta = 0$ is ~ 6 times higher than for $\eta = 10^{-6}$, while the velocity of the pair plasma is ~ 6 times smaller. This is because for a surface temperature $T_S \simeq 4 \times 10^8$ K, which corresponds to $\tilde{L}_\pm = 10^{34}$ ergs s $^{-1}$, the mean kinetic energy of pairs near the surface, $(3/2)k_B T_S \simeq 8.3 \times 10^{-8}$ ergs is about half of the gravitational binding energy, so an atmosphere may form. In addition, for low surface photon luminosities ($\eta \lesssim$ a few $\times 10^{-8}$) radiation pressure is too weak to suppress the plasma atmosphere that results from the presence of gravity. So, an atmosphere does form, and, in turn, is conducive to pair annihilation. In contradistinction for $\eta = 10^{-6}$ radiation pressure does suppress the formation of an atmosphere, and the pair wind structure, i.e., the runs of $n_e(r)$ and $v_e^{\text{out}}(r)$, is very similar to the case with no gravity and $\eta = 0$.

Figure 5 shows the rates of outflow of e^\pm pairs (\dot{N}_\pm) and photons (\dot{N}_γ) through the surface as functions of r . For high luminosities ($\tilde{L}_\pm \gtrsim 10^{37}$ ergs s $^{-1}$) the rate of pair outflow \dot{N}_\pm almost doesn't depend on η and decreases significantly at the distance

$$l_{\text{ann}} \simeq 10 \left(\frac{\tilde{L}_\pm}{10^{39} \text{ ergs s}^{-1}} \right)^{-1} \text{ cm} \quad (35)$$

from the stellar surface because of pair annihilation (see the estimate of l_{ann} in Paper I). For low luminosities ($\tilde{L}_\pm \lesssim 10^{35}$ ergs s $^{-1}$) the dependence of \dot{N}_\pm on r is different for different values of η . For $\eta = 0$ the value of \dot{N}_\pm decreases outwards at least by a factor of 2 even when

\tilde{L}_\pm is as small as 10^{34} ergs s^{-1} , while for $\eta = 10^{-6}$ the decrease of \dot{N}_\pm due to pair annihilation is very small for low luminosities, again reflecting the degree to which a pair atmosphere is formed.

The photon outflow rate is seen to increase with increasing r not only because of pair annihilation, but also because of accumulative production of photons by radiative three-body processes. These processes are important for high luminosities ($\tilde{L}_\pm \gtrsim 10^{38}$ ergs s^{-1}) and are responsible for the increase of \dot{N}_γ at $r - R \sim 10^3 - 10^5$ cm for such high luminosities (see Fig. 5).

The rates of energy outflow in e^\pm pairs (\dot{E}_\pm) and photons (\dot{E}_γ) vary with radius more or less similarly to the particle outflow rates, except that the total energy rate is explicitly conserved in all processes (see Fig. 6). The total energy rate decreases with increase of r because of the gravity effects,

$$\dot{E}(r) = \dot{E}_\pm(r) + \dot{E}_\gamma(r) = e^{2(\tilde{\phi}-\phi)} \tilde{L} = \frac{1 - r_g/R}{1 - r_g/r} \tilde{L}, \quad (36)$$

and varies from $\tilde{L} = \tilde{L}_\pm + \tilde{L}_\gamma$ at $r = R$ to the total emerging luminosity

$$L = L_\pm + L_\gamma = \dot{E}(r_{\text{ext}}) = \frac{1 - r_g/R}{1 - r_g/r_{\text{ext}}} \tilde{L} \quad (37)$$

at $r = r_{\text{ext}}$. This differs qualitatively from Paper I where the gravity effects are ignored, and $\dot{E}(r)$ is constant.

The number rates of emerging pairs (\dot{N}_\pm) as functions of \tilde{L}_\pm for different values of η are shown in Figure 7. For $\tilde{L}_\pm = 10^{34}$ ergs s^{-1} the value of \dot{N}_\pm for $\eta = 0$ is ~ 3 times smaller than the same for $\eta = 10^{-6}$. The results of our new simulations for $\eta = 10^{-6}$ and our old simulations with $\eta = 0$ and no gravity practically coincide. This is consistent with our results on the wind structure. For $\tilde{L}_\pm \gtrsim 10^{37}$ ergs s^{-1} \dot{N}_\pm hardly depends on η , and is $\sim 1.5 - 2$ times smaller than the result of Paper I (see Fig. 7). This is due to partial suppression of pair creation as the photon energies are reduced by gravitational redshift.

Figure 8 shows the emerging total luminosities in e^\pm pairs (L_\pm , including the rest mass) and photons (L_γ)—given as fractions of the total emerging luminosity $L = L_\pm + L_\gamma$ —as functions of the injection luminosity, and for different values of η . For the luminosity range we consider photons dominate in the emerging emission ($L_\gamma > L_\pm$), especially at high luminosities where $L_\gamma \gg L_\pm$.

Figure 9 presents the energy spectra of the emerging photons for different values of \tilde{L}_\pm and η . For low luminosities ($\tilde{L}_\pm \lesssim 10^{36}$ ergs s^{-1}) and $\eta = 0$, photons, which form by pair annihilation, escape more or less freely from the star's vicinity, and the photon spectra

represent a very wide annihilation line that is redshifted in the gravitational field. The mean energy of the emerging photons varies from ~ 430 keV for $\tilde{L}_{\pm} = 10^{34}$ ergs s $^{-1}$ to 400 keV for $\tilde{L}_{\pm} = 3 \times 10^{36}$ ergs s $^{-1}$ (see Fig. 10). If η is near its maximum value ($\sim 10^{-6}$) there is no annihilation line in the spectra of emerging photons. Annihilation photons only modify these spectra by producing high-energy tails (see Fig. 9c). For high luminosities ($\tilde{L}_{\pm} \gtrsim 10^{38}$ ergs s $^{-1}$) the energy spectra of emerging photons practically don't depend on η and coincide with the results of Paper I.

5. Discussion

We have identified certain characteristics of pair winds outflowing from hot, bare, strange stars and their emerging emission. For the energy injection rate in pairs we consider ($\tilde{L}_{\pm} = 10^{34} - 10^{39}$ ergs s $^{-1}$) photons dominate in the emerging emission (see Fig. 8.). The spectrum of the emerging photons, we find, is rather hard (see Figs. 9 and 10) and differs qualitatively from the spectrum of the thermal emission from a neutron star with the same luminosity (e.g., Romani 1987; Shibano et al. 1992; Rajagopal & Romani 1996; Page et al. 2004). In particular, for a bare strange star the mean energy of the emerging photons (see Fig. 10) is at least an order of magnitude larger than the same for a neutron star. This opens observational possibilities to distinguish strange stars from neutron stars. Hard spectra of bare strange stars are amenable to detection and study by sensitive, hard X-ray and soft γ -ray instruments, such as *INTEGRAL* (e.g., Winkler et al. 2003).

In this study we take into account both the thermal emission of photons from the strange star surface and gravity that have been neglected in Paper I. We have shown that for low values of $\eta \lesssim$ a few $\times 10^{-8}$ and $\tilde{L}_{\pm} \lesssim 10^{35}$ ergs s $^{-1}$ pairs emitted by the stellar surface are mainly captured by the gravitational field, and a pair atmosphere forms. The probability of pair annihilation increases because of the increase of the pair number density in the atmosphere, and this results in decrease of the fraction of pairs in the emerging emission in comparison with the case of Paper I (see Figs. 7 and 8). However, if the surface emission in photons is as high as its upper limit ($\eta \simeq 10^{-6}$) radiation pressure forces dominate over gravity, and the pair wind structure practically coincides with the results for no gravity, irrespective of \tilde{L}_{\pm} .

The dominant physical processes in pair winds change significantly depending on \tilde{L}_{\pm} . For $\tilde{L}_{\pm} < L_* \simeq 10^{37}$ ergs s $^{-1}$ the optical depth for photons is smaller than unity, $\tau_{\gamma} < 1$ (see Fig. 2). In this case some part of e^{\pm} pairs ejected from the stellar surface annihilates into photons in the process of their outflow, while photo-creation of pairs is rather rare. Above $\tilde{L}_{\pm} \simeq L_*$ pair creation by photons becomes important, and for $\tilde{L}_{\pm} \gg L_*$ the rates of pair

creation and pair annihilation are more or less comparable at $l_{\text{ann}} \lesssim r - R \ll r_{\text{ph}}$. At such distances from the surface the number density of pairs is nearly constant (see Fig. 3 and Fig. 8 in Paper I). In addition, for high luminosities ($\tilde{L}_{\pm} \gtrsim 10^{38}$ ergs s $^{-1}$) radiative three-body processes are important, and the total rate of the particle outflow increases with radius (see Fig. 5). These processes favour thermalization of pairs and photons in the outflow.

For low luminosities ($\tilde{L}_{\pm} < L_*$) the spectrum of emerging photons significantly depends on the photo-emission from the surface, especially at low energies, $\epsilon_{\gamma} \ll m_e c^2$ (see Fig. 9). If surface photo-emission is negligible ($\eta = 0$), this spectrum resembles a very wide annihilation line. The fractional emerging luminosity in the annihilation line decreases with the increase of η . For $\eta = 10^{-6}$ the annihilation line is completely washed out, and a high-energy part of this line is observed as a high-energy tail (see Fig. 9c). For high luminosities ($\tilde{L}_{\pm} \gtrsim 10^{38}$ ergs s $^{-1}$) the spectrum of emerging photons is practically independent of the photon emission from the stellar surface.

Soft γ -ray repeaters (SGRs), which are the sources of short bursts of hard X-rays with super-Eddington luminosities (up to $\sim 10^{42} - 10^{47}$ ergs s $^{-1}$), are potential candidates for strange stars (e.g., Alcock et al. 1986b; Cheng & Dai 1998; Usov 2001c; Ouyed et al. 2005). The bursting activity of SGRs may be explained by fast heating of the stellar surface up to a temperature of $\sim (1 - 3) \times 10^9$ K and its subsequent thermal emission (Usov 2001b,c). The heating mechanism may be either impacts of comets onto bare strange stars (Zhang et al. 2000; Usov 2001b) or fast decay of superstrong ($\sim 10^{14} - 10^{15}$ G) magnetic fields (Thompson & Duncan 1995; Heyl & Kulkarni 1998). Since for high luminosities ($\gtrsim 10^{38}$ ergs s $^{-1}$) the spectrum of emerging photons practically doesn't depend on the surface photo-emission, which is poorly known, it is possible to calculate more securely many properties (light curves, energy spectra, etc.) of powerful ($L \gg 10^{38}$ ergs s $^{-1}$) X-ray bursts expected from the stellar surface heating neglecting surface photo-emission. We plan to apply the tools developed here to study these problems.

We thank members of the Israeli Center for High Energy Astrophysics, D. Eichler, A. Levinson, T. Piran, and E. Waxman, for helpful discussions. The research was supported by the Israel Science Foundation of the Israel Academy of Sciences and Humanities.

REFERENCES

- Aksenov, A.G. 1998, *Astron. Lett.*, 24, 482
- Aksenov, A.G., Milgrom, M., & Usov, V.V. 2003, *MNRAS*, 343, L69
- Aksenov, A.G., Milgrom, M., & Usov, V.V. 2004, *ApJ*, 609, 363 (Paper I)
- Alcock, C., Farhi, E., & Olinto, A. 1986a, *ApJ*, 310, 261
- Alcock, C., Farhi, E., & Olinto, A. 1986b, *Phys. Rev. Lett.*, 57, 2088
- Arons, J. 1981, *ApJ*, 248, 1099
- Baring, M.G., & Harding, A.K. 2001, *ApJ*, 547, 929 M.C.,
- Beloborodov, A.M. 1999, *MNRAS*, 305, 181
- Cheng, K.S., & Dai, Z.G. 1998, *Phys. Rev. Lett.*, 80, 18
- Cheng, K.S., & Harko, T. 2003, *ApJ*, 596, 451
- Chmaj, T., Haensel, P., & Słomiński, W. 1991, *Nucl. Phys. B*, 24, 40
- Eichler, D., Livio, M., Piran, T., & Schramm, D. 1989, *Nature*, 340, 126
- Goodman, J. 1986, *ApJ*, 308, L47
- Grimsrud, O.M., & Wasserman, I. 1998, *MNRAS*, 300, 1158
- Haensel, P., Zdunik, J.L., & Schaeffer, R. 1986, *ApJ*, 160, 121
- Hall, G., & Watt, J.M. 1976, *Modern Numerical Methods for Ordinary Differential Equations* (Oxford: Clarendon Press)
- Harleston, H., & Holcomb, K.A. 1991, *ApJ*, 372, 225
- Harleston, H., & Vishniac, E.T. 1992, *Phys. Rev. D*, 45, 4458
- Heyl, J.S., & Kulkarni, S.R. 1998, *ApJ*, 506, L61
- Iwamoto, S., & Takahara, F. 2002, *ApJ*, 565, 163
- Jaikumar, P., Gale, C., Page, D., & Prakash, M. 2004, *Phys. Rev. D*, 70, 023004
- Kettner, Ch., Weber, F., Weigel, M.K., & Glendenning, N.K. 1995, *Phys. Rev. D*, 51, 1440

- Melrose, D.B. 1995, *JA&A*, 16, 137
- Mezzacappa, A., & Bruenn, S.W. 1993, *ApJ*, 405, 669
- Ouyed, R., Rapp, R., & Vogt, C. 2005, astro-ph/0503357
- Paczynski, B. 1986, *ApJ*, 308, L43
- Paczynski, B. 1990, *ApJ*, 363, 218
- Page, D., Lattimer, J.M., Prakash, M., & Steiner, A.W. 2004, *ApJS*, 155, 623
- Page, D., & Usov, V.V. 2002, *Phys. Rev. Lett.*, 89, 131101
- Piran, T. 2000, *Phys. Rep.*, 333, 529
- Rajagopal, M., & Romani, R.W. 1996, *ApJ*, 461, 327
- Richtmeyer, R., & Morton, K. 1967. *Difference Methods for Initial Value Problems* (New York: Wiley-Interscience)
- Romani, R.W. 1987, *ApJ*, 313, 718
- Ruderman, M.A., & Sutherland, P.G. 1975, *ApJ*, 196, 51
- Schwinger, J. 1951, *Phys. Rev.*, 82, 664
- Shibanov, Yu.A., Zavlin, V.E., Pavlov, G.G., and Ventura, J. 1992, *A&A*, 266, 313
- Sturrock, P.A. 1971, *ApJ*, 164, 529
- Sunyaev, R.A., et al. 1992, *ApJ*, 389, L75
- Thompson, C. & Duncan, R.C. 1995, *MNRAS*, 275, 255
- Usov, V.V. 1992, *Nature*, 357, 472
- Usov, V.V. 1998, *Phys. Rev. Lett.*, 80, 230
- Usov, V.V. 2001a, *ApJ*, 550, L179
- Usov, V.V. 2001b, *Phys. Rev. Lett.*, 87, 021101
- Usov, V.V. 2001c, *ApJ*, 559, L138
- Usov, V.V. 2004, *Phys. Rev. D*, 70, 067301

Usov, V.V., Harko, T., & Cheng, K.S. 2005, ApJ, 620, 915

Usov, V.V., & Melrose, D.B. 1996, ApJ, 464, 306

White, T.R., & Lightman, A.P. 1989, ApJ, 340, 1024

Winkler, C. et al. 2003, A&A, 411, L349 T.,

Zhang, B., Xu, R.X., & Qiao, G.J. 2000, ApJ, 545, L127

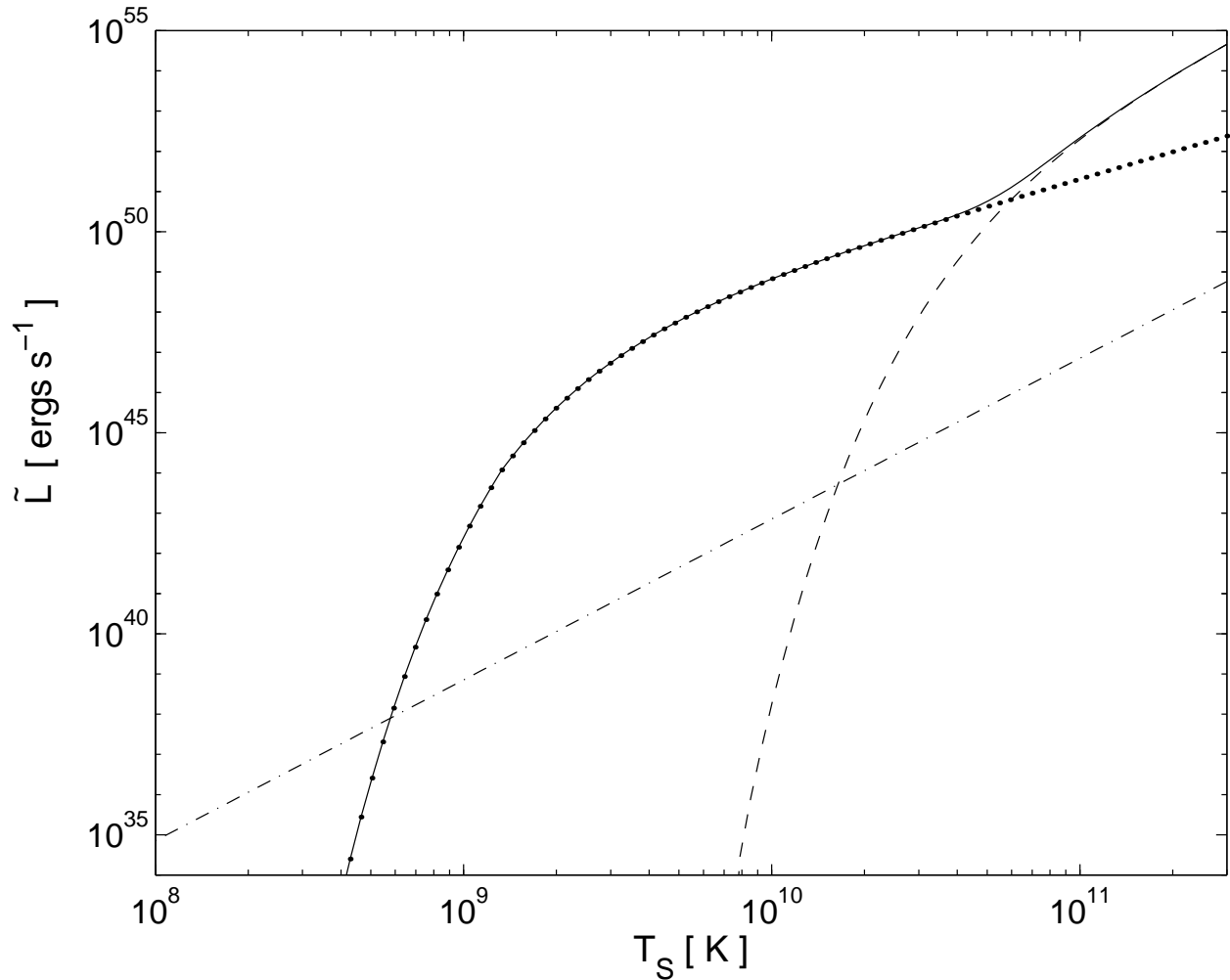


Fig. 1.— Injection luminosities of a hot, bare, strange star in e^+e^- pairs (dotted line), in thermal equilibrium photons (dashed line), and the total (solid line) as functions of the surface temperature T_s . The theoretical upper limit on the luminosity in non-equilibrium photons, $10^{-6}L_{\text{BB}}$ (Cheng & Harko 2003), is shown by the dot-dashed line, L_{BB} being the blackbody luminosity.

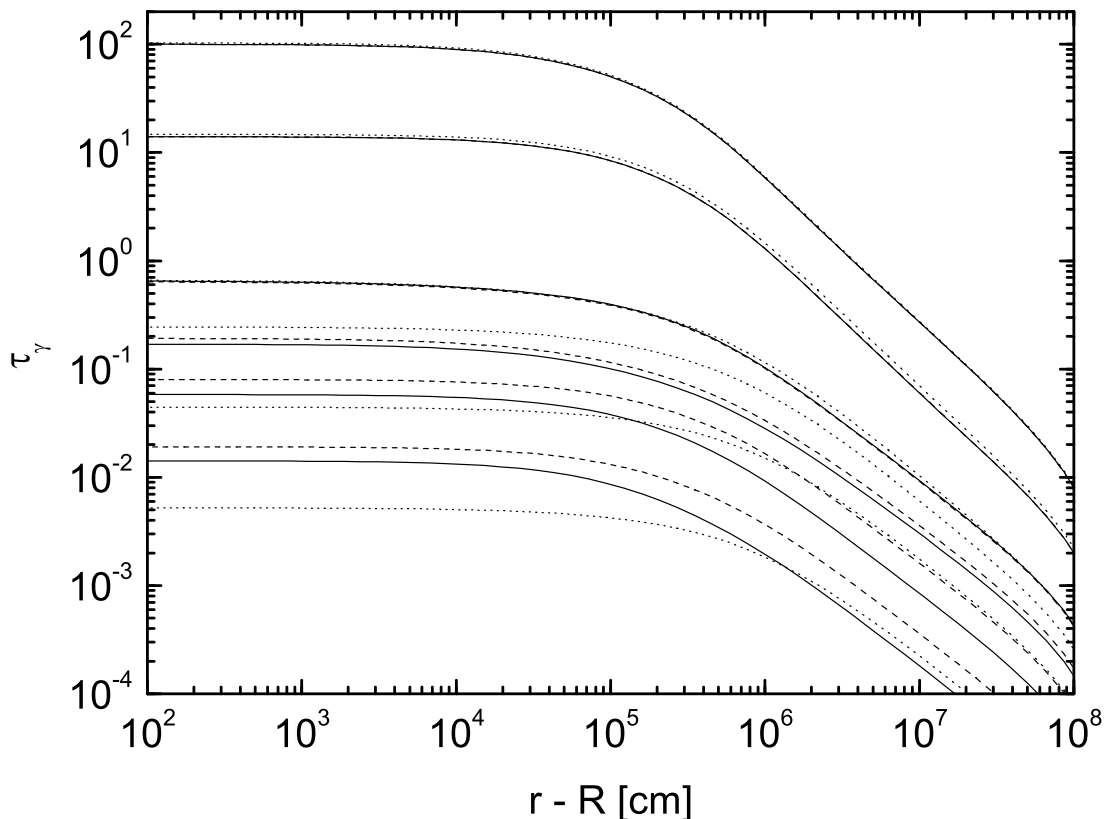


Fig. 2.— Mean optical depth for photons, from r to infinity, as a function of the distance from the stellar surface for $\eta = 0$ (solid lines), $\eta = 3 \times 10^{-8}$ (dashed lines), and $\eta = 10^{-6}$ (dotted lines), and for different values of the injected pair luminosity, \tilde{L}_{\pm} , which increases in steps of factor ten from 10^{34} ergs s^{-1} (lowest triplet of lines) to 10^{39} ergs s^{-1} (uppermost triplet of practically coinciding lines).

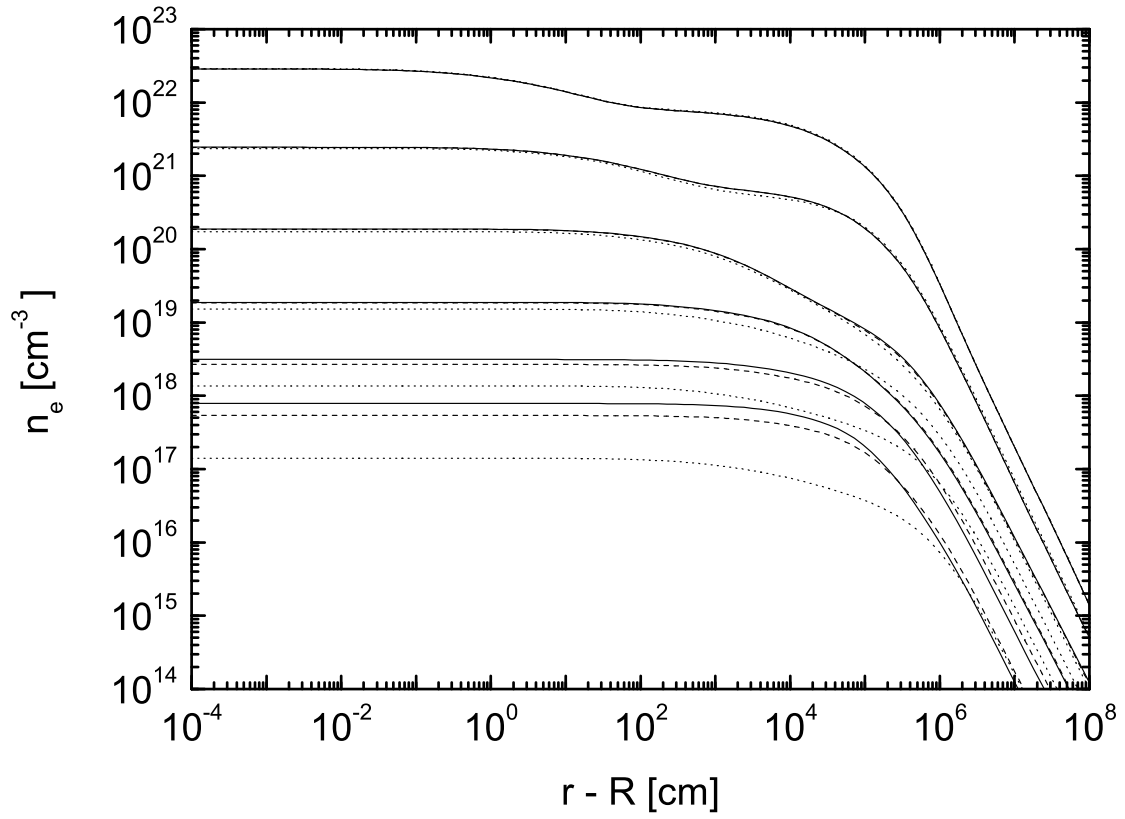


Fig. 3.— Pair number density as a function of the distance from the stellar surface, line designation as in Fig. 2.

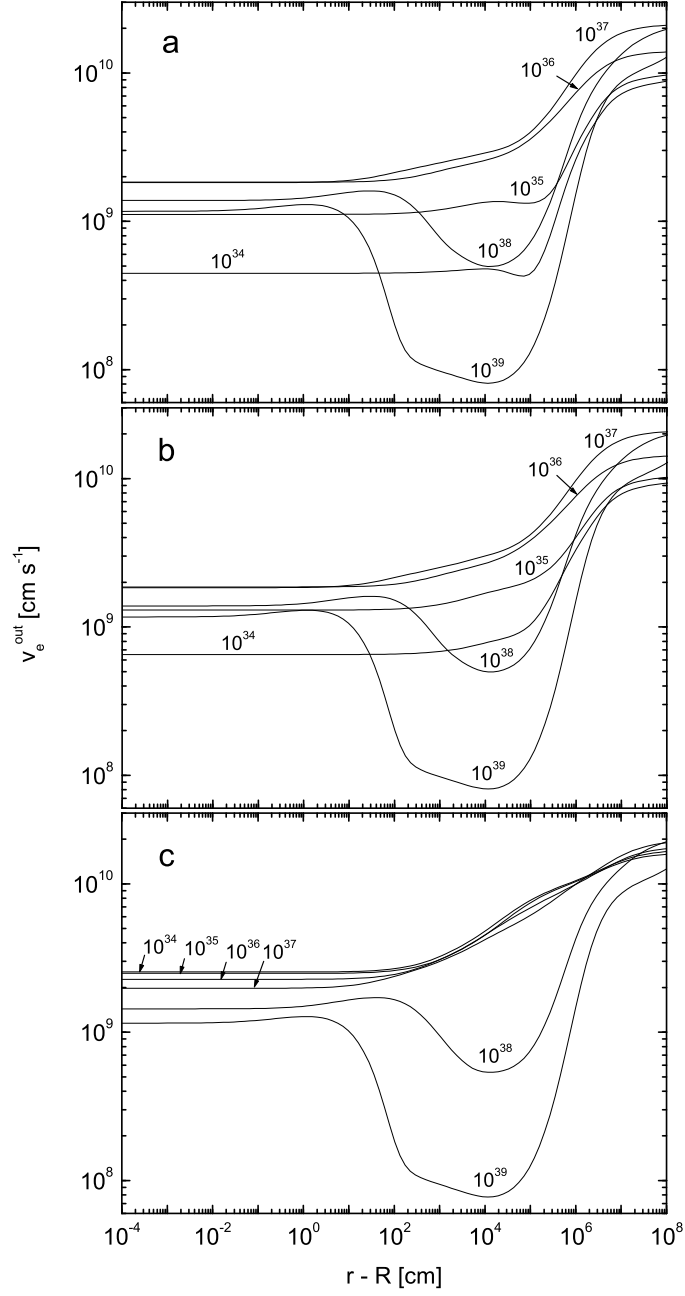


Fig. 4.— Bulk velocity of the pair plasma as a function of the distance from the stellar surface for (a) $\eta = 0$, (b) $\eta = 3 \times 10^{-8}$, and (c) $\eta = 10^{-6}$, shown for different values of \tilde{L}_{\pm} , as marked on the lines.

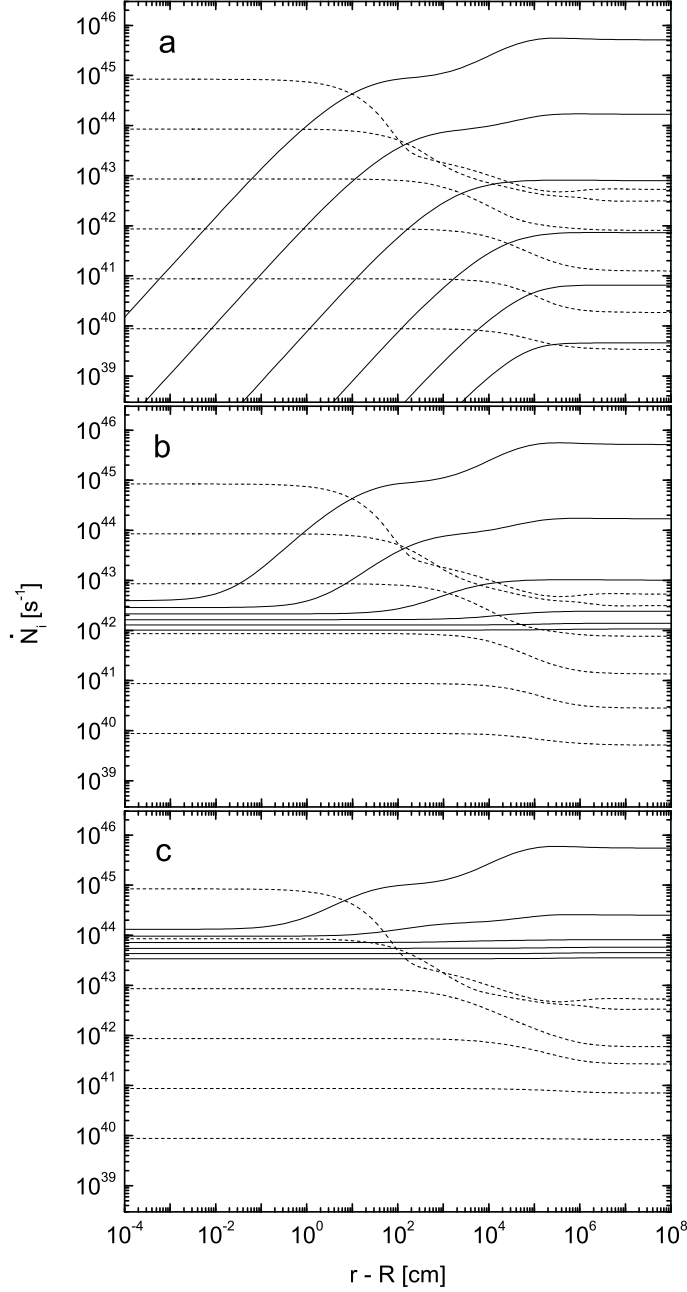


Fig. 5.— Particle number outflow rates in photons (solid lines) and e^\pm pairs (dashed lines) as functions of the distance from the stellar surface for (a) $\eta = 0$, (b) $\eta = 3 \times 10^{-8}$, and (c) $\eta = 10^{-6}$, shown for different values of \tilde{L}_\pm , which increases in steps of factor ten from 10^{34} ergs s^{-1} (lowest lines for each species) to 10^{39} ergs s^{-1} (uppermost lines).

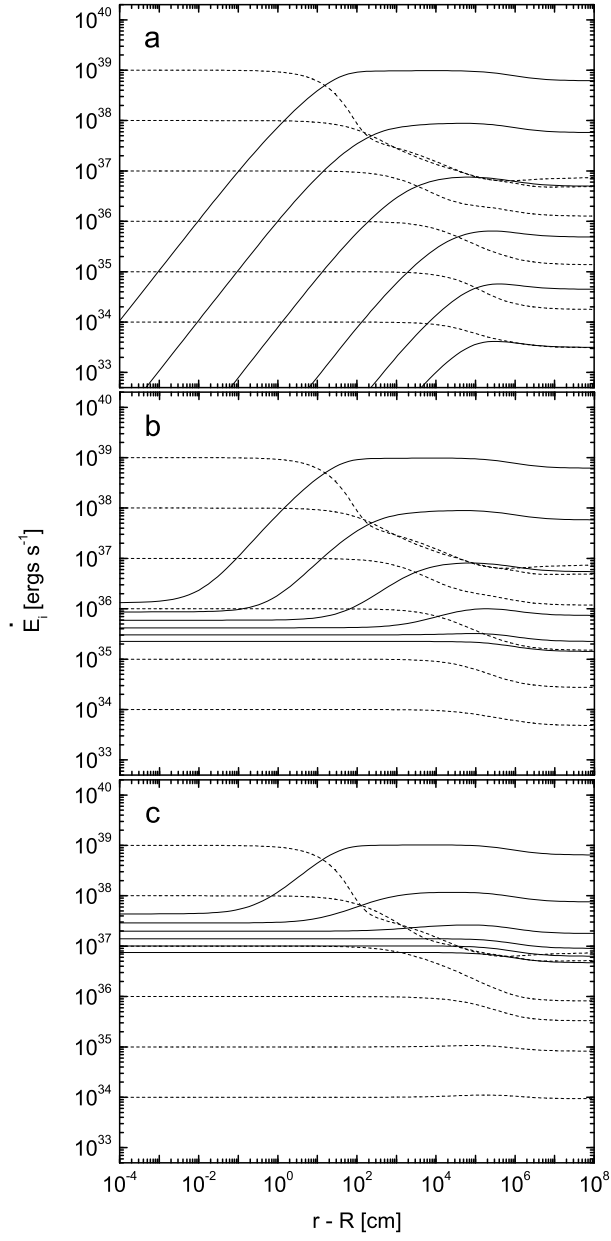


Fig. 6.— Rates of energy outflow, as in Fig. 5.

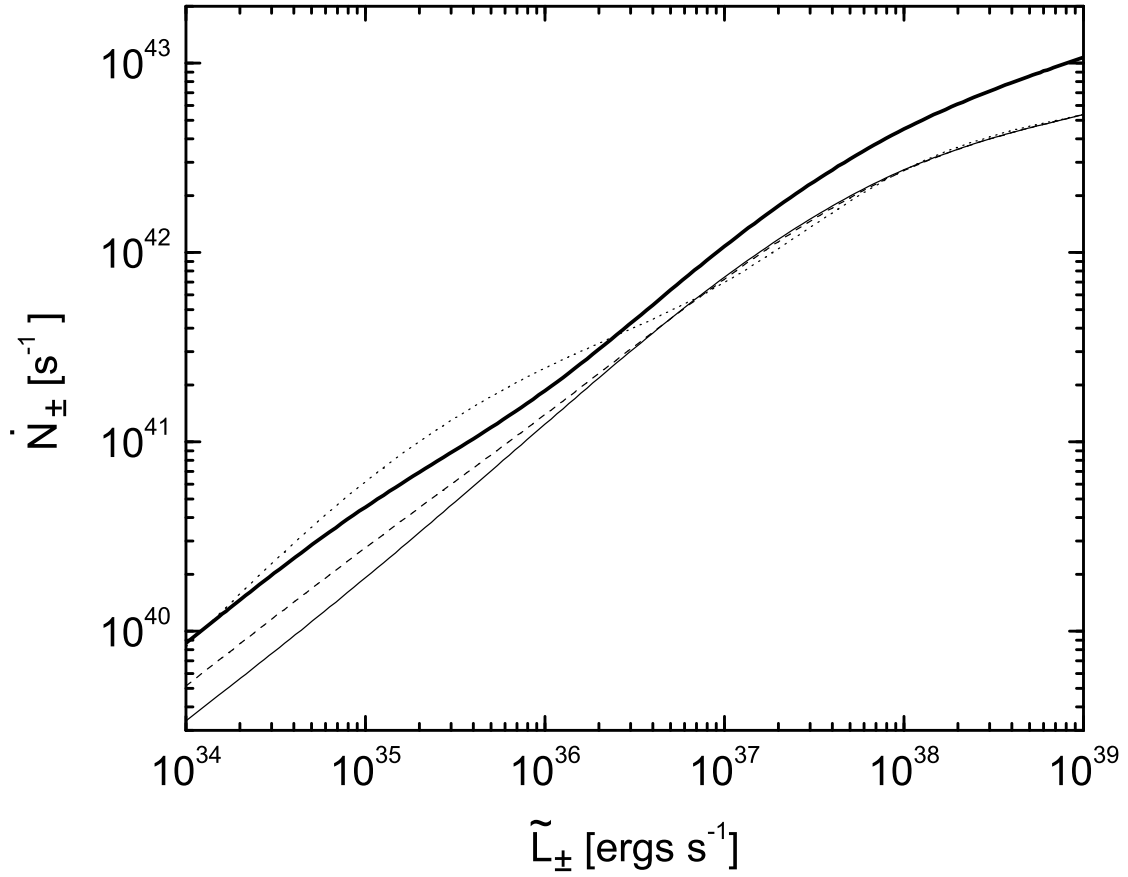


Fig. 7.— Number rates of emerging pairs as functions of the injected pair luminosity for $\eta = 0$ (thin solid line), $\eta = 3 \times 10^{-8}$ (dashed line), $\eta = 10^{-6}$ (dotted line). The result of Paper I where gravity has been neglected and $\eta = 0$ is shown by the thick solid line.

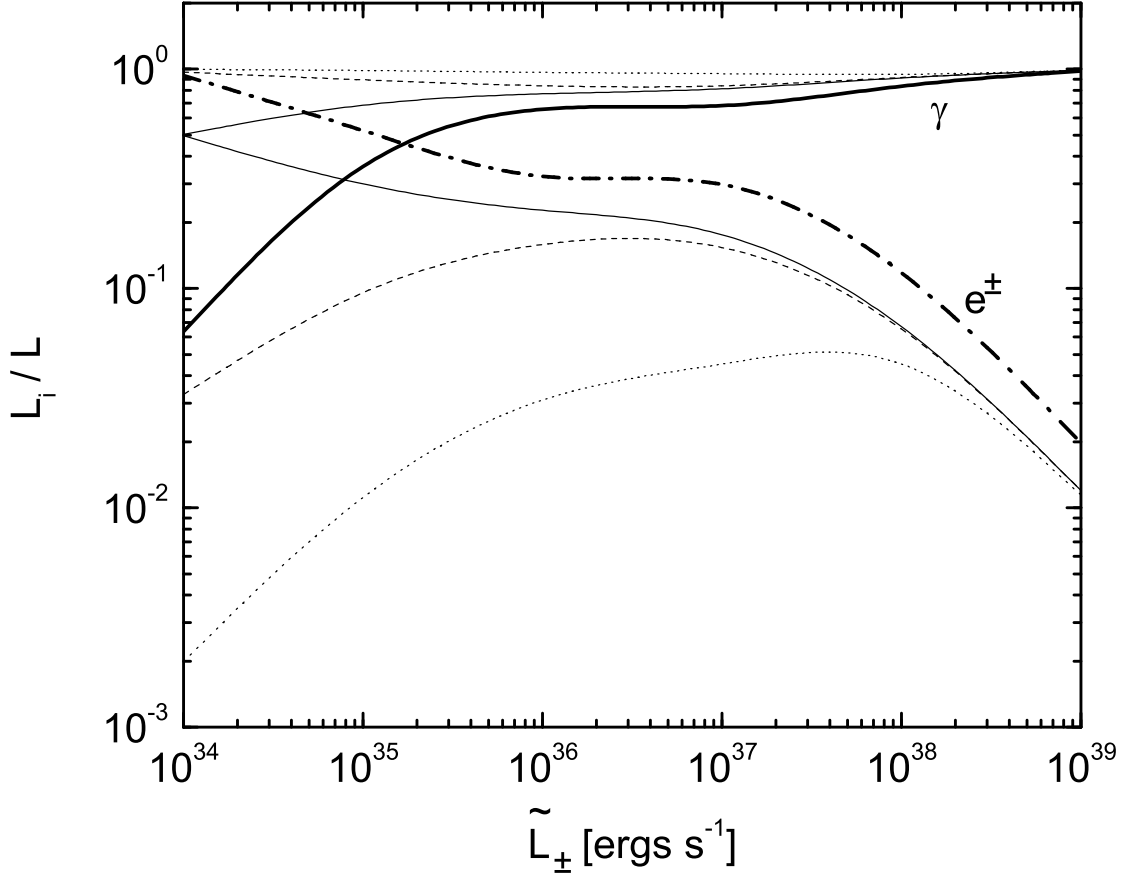


Fig. 8.— Fractional emerging luminosities in photons (upper triplet of thin lines) and pairs (lower triplet of thin lines) as functions of the injected pair luminosity for $\eta = 0$ (thin solid lines), $\eta = 3 \times 10^{-8}$ (dashed lines), and $\eta = 10^{-6}$ (dotted lines). The results for the case where gravity is neglected and $\eta = 0$ are shown for comparison by thick solid line and thick dot-dashed line for emerging photons and emerging pairs, respectively.

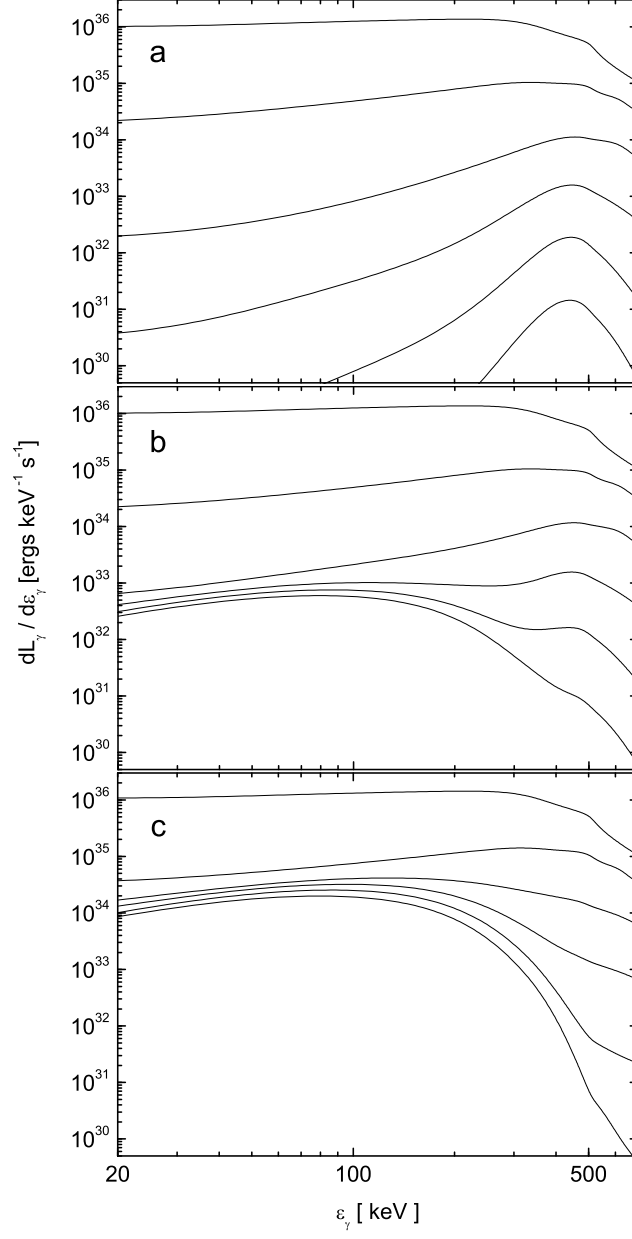


Fig. 9.— Energy spectrum of emerging photons for (a) $\eta = 0$, (b) $\eta = 3 \times 10^{-8}$, and (c) $\eta = 10^{-6}$, shown for different values of \dot{L}_{\pm} , which increases in steps of factor ten from 10^{34} ergs s^{-1} (lowest lines) to 10^{39} ergs s^{-1} (uppermost lines).

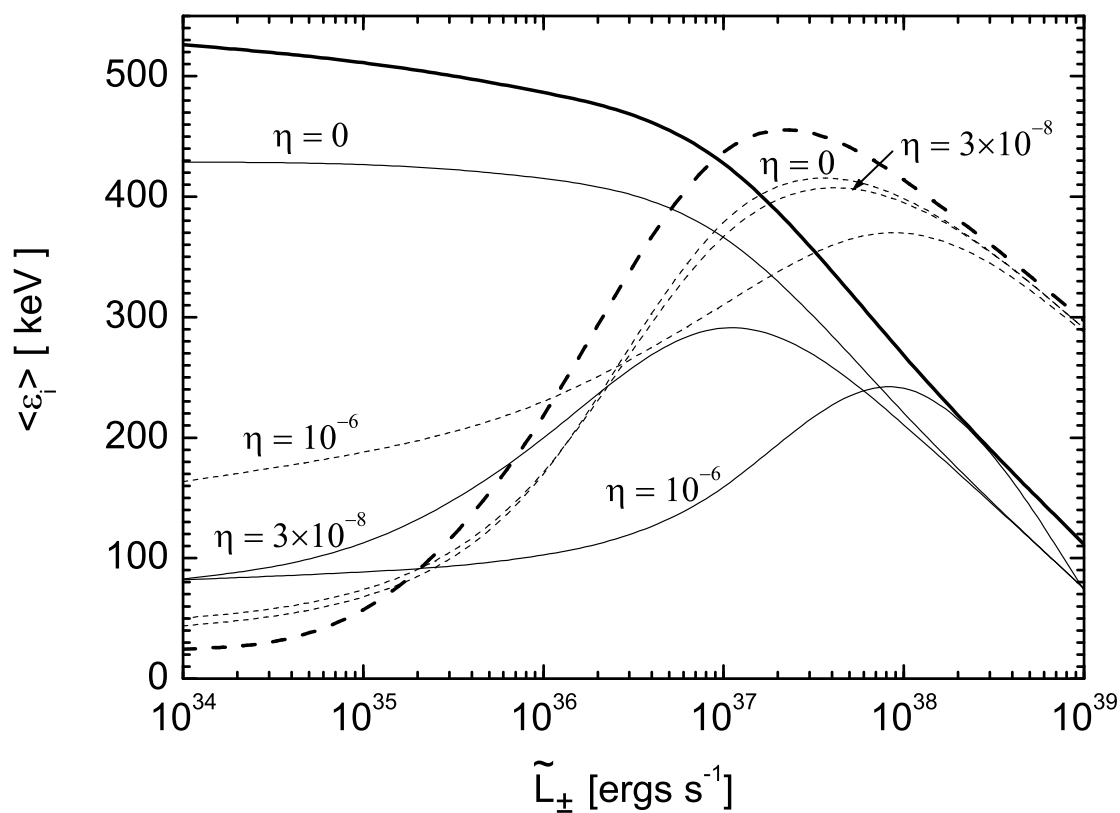


Fig. 10.— Mean energy of the emerging photons (thin solid lines) and electrons (thin dashed lines) as functions of the injected pair luminosity for different values of η , as marked on the lines. The results of Paper I where $\eta = 0$ and no gravity are shown by the thick solid and thick dashed lines for photons and electrons, respectively.